Colloids and Surfaces B: Biointerfaces 161 (2018) 375–385

Contents lists available at ScienceDirect

Colloids and Surfaces B: Biointerfaces

journal homepage: www.elsevier.com/locate/colsurfb

Protocols

Study of rabbit erythrocytes membrane solubilization by sucrose monomyristate using laurdan and phasor analysis

German Günther[a], Vanesa Herlax[b], M. Pilar Lillo[c], Catalina Sandoval-Altamirano[a], Libnny N. Belmar[d], Susana A. Sánchez[d,*]

[a] Laboratorio de Cinética y Fotoquímica, Facultad de Ciencias Químicas y Farmacéuticas, Universidad de Chile, Santiago, Chile
[b] Instituto de Investigaciones Bioquímicas de La Plata (INIBIOLP), CCT—La Plata, CONICET, Facultad de Ciencias Médicas, Universidad Nacional de La Plata, La Plata, Argentina
[c] Departamento de Química Física Biológica, Instituto de Química-Física Rocasolano. (CSIC), Madrid, Spain
[d] Universidad de Concepción, Facultad de Ciencias Químicas, Departamento de Polímeros, Concepción, Chile

ARTICLE INFO

Article history:
Received 5 August 2017
Received in revised form 6 October 2017
Accepted 30 October 2017
Available online 1 November 2017

Keywords:
FLIM phasor
Spectral phasor
Laurdan GP
Solubilization
Surfactants
Sucrose ester
Membrane heterogeneity
Membrane fluidity

ABSTRACT

The study of surfactant and bio membranes interaction is particularly complex due to the diversity in lipid composition and the presence of proteins in natural membranes. Even more difficult is the study of this interaction in vivo since cellular damage may complicate the interpretation of the results, therefore for most of the studies in this field either artificial or model systems are used. One of the model system most used to study biomembranes are erythrocytes due to their relatively simple structure (they lack nuclei and organelles having only the plasma membrane), their convenient experimental manipulation and availability.

In this context, we used rabbit erythrocytes as a model membrane and Laurdan (6-lauroyl-2-dimethylaminonaphthalene) as the fluorescent probe to study changes promoted in the membrane by the interaction with the sucrose monoester of myristic acid, β-D-fructofuranosyl-6-*O*-myristoyl-α-D-glucopyranoside (MMS). Surfactant and erythrocytes interaction was studied by measuring hemoglobin release and the changes in water content in the membrane sensed by Laurdan. Using two-photon excitation, three types of measurements were performed: Generalized Polarization (analyzed as average GP values), Fluorescence Lifetime Imaging, FLIM (analyzed using phasor plots) and Spectral imaging (analyzed using spectral phasor). Our data indicate that at sublytical concentration of surfactant (20 μM MMS), there is a decrease of about 35% in erythrocytes size, without changes in Laurdan lifetime or emission spectra. We also demonstrate that as hemolysis progress, Laurdan lifetime increased due to the decrease in hemoglobin (strong quencher of Laurdan emission) content inside the erythrocytes. Under these conditions, Laurdan spectral phasor analyses can extract the information on the water content in the membrane in the presence of hemoglobin. Our results indicate an increase in membrane fluidity in presence of MMS.

1. Introduction

Solubilization of membranes by surfactants is a well-known method used to understand the nature and properties of the cellular bilayer and its components. The use of micelle-forming surfactants is one of the preferred methods for isolation of specific membrane constituents [1–3]. Several articles in the literature describe in detail the interaction of surfactants with artificial membranes [4–7]; however, this is not the case concerning the interaction of surfactants with biological membranes, where the lipid composition diversity and the presence of proteins make the scenario more complex.

Biological bilayers are complex, with membrane lateral heterogeneity being accepted as a requirement for their function and the notion of lipid rafts supporting that concept [8]. The operational definition of rafts came from the observation of membrane resistance to solubilization with nonionic detergents like Triton X-100 at 4 °C. Since in these assays a fraction of the membranes remained insoluble, the suggestion was made that these detergent-resistant membranes (DRMs) corresponded to supramolecular entities floating in fluid biological membranes as *rafts* [9]. However, it is commonly accepted that DRMs are produced by the reorganiza-

* Corresponding author.
E-mail address: susanchez@udec.cl (S.A. Sánchez).

https://doi.org/10.1016/j.colsurfb.2017.10.068
0927-7765/

tion of lipids and proteins upon the addition of detergent and they do not correspond to rafts in vivo [10,11]. Because of these observations, the concepts of rafts and DRMs should be used with extreme caution [12]. The actual definition of *rafts* correspond to structures existing in vivo that are sterol and sphingolipid-enriched, with small size (10–200 nm), heterogeneous and highly dynamic [13]. The solubilization process in bio membranes may be different depending on the state of this structures, in fact, the presence of cholesterol in lipid mixtures makes the bilayers more resistant to solubilization [14], and in equimolar mixtures with phosphatidylcholine, cholesterol decreased the stability of the bilayer towards Triton X-100 [15].

Erythrocytes are the most commonly used model system to study bio membranes due to their relatively simple structure: they lack nuclei and organelles, having only the plasma membrane. However, the presence of membrane lipid domains in erythrocytes has been reported using different approaches [16–20]. In studies involving erythrocyte/surfactant interaction, two parameters are normally studied: permeability and structural changes of the membrane. Permeability changes are followed by hemoglobin release, and membrane structural properties are monitored by different techniques such as fluorescence of specific dyes [21,22], spin labeling [23], scanning calorimetry, NMR and Fourier-transform infrared spectroscopy [24] among others. In erythrocytes, membrane solubilization may occur in parallel with hemolysis. Preté et al. reported [25] the use of the hemolysis curve (obtained from the interaction of Triton X-100 with erythrocytes) to obtain membrane structural parameters by applying the analysis of membrane solubilization proposed by Lichtenberg [26–28]. Thus, the beginning of hemolysis would be an indication of achievement of bilayer saturation (C^{sat}) and the end of hemolysis would correspond to the concentration of detergent for total membrane solubilization (C^{sol}).

In the present study, we report the interaction of rabbit erythrocytes with the sucrose monoester, β-D-fructofuranosyl-6-*O*-myristyl-α-D-glucopyranoside (Mono myristoyl sucrose, MMS) using two-photon excitation fluorescent microscopy. Sucrose esters correspond to a class of nonionic detergents that are non-toxic, skin compatible, non-polluting and biodegradable. Derivatives of stearic acid had been employed for the extraction of cytochrome and lysozyme [29–31] and their capability to solubilize different synthetic membranes has been reported by our group [2,6]. As a fluorescent dye we used Laurdan ((6-lauroyl-2-dimethylaminonaphthalene)), a molecule widely used to study membrane properties both in artificial [32,33] and natural systems, in cuvette [7,22] and under the microscope [2,34]. Laurdan Lifetime and spectral images were analyzed using the phasor method [35–37]. We followed hemoglobin release and changes in the membrane properties of erythrocytes after interaction with MMS. Hemoglobin release was measured by colorimetric and biochemical methods and membrane properties were observed by bright-field and two-photon excitation fluorescence microscopy.

2. Material and methods

2.1. Samples

Rabbit blood samples were purchased from Colorado Serum Company (Denver, CO, USA). Sucrose monoester, β-D-fructofuranosyl-6-*O*-myristyl-α-D-glucopyranoside (MMS, Mono myristyl sucrose, C14) was synthesized by a modification of the Vlahov method [38] where the relation between sucrose complex and acyl chloride was changed from two to one. The reaction yields a mixture of monoesters (mainly 6-O and presumably a small quantity of 1-O), accompanied with low amounts of di- and tri-esters. Pure 6-O monoester was obtained by chromatography on silica column. For solubilization experiments with erythrocytes, a stock solution of MMS in PBS-saline buffer (10 mM Na_2PO_4 pH 7.5, containing 147 mM NaCl and 3 mM KCl) was prepared. Laurdan was purchased from Invitrogen (Thermos Fisher Scientific).

2.2. Preparation of erythrocytes and ghosts

Freshly defibrinated rabbit blood (Colorado Company) was used in all the solubilization experiment. Blood, received the same day it was drawn, was stored at 4 °C and the whole erythrocyte experiments were performed the same day. Rabbit erythrocytes (RRBC), were centrifuged at 4000 rpm (1800*g*), rinsed and suspended to the original hematocrit (40% vol/vol) in PBS-saline buffer. Erythrocytes (at final hematocrit of 5% vol/vol) were incubated with different concentrations of the detergent in PBS for 1 h at 37 °C. After incubation, erythrocytes were centrifuged at 4000 rpm (1800*g*), and hemoglobin determination (absorbance at 410 nm) and protein released from the membrane (gradient 5–20% native PAGE) were determined in the supernatant. Pellet was rinsed three times with PBS for the fluorescence imaging measurements. Detergent-treated erythrocytes were diluted with PBS to hematocrit 0.2% vol/vol and incubated with 1 μM Laurdan for 30 min at 37 °C. For microscope observation, samples were deposited in a microscope dish coated with poly-lysine (MatTek Co. Ashland, MA, USA) to allow the adhesion of the erythrocytes to the dish. Measurements under the microscope (fluorescence and transmission) were obtained at 37 °C in a temperature-controlled stage.

Ghost erythrocytes were prepared using a modified protocol published by Dodge et al. [20]. Briefly, erythrocytes were lysed with an hypotonic buffer (1 mM PBS pH 7.4) during 30 min at 4 °C. Then ghost membranes were separated by centrifugation at 14,000 rpm (22000*g*) for 10 min at 4 °C. This procedure was repeated until the samples were free of hemoglobin.

2.3. SDS – PAGE to study protein released from treated-erythrocytes membranes with MMS

Fifteen μl of the supernatant obtained after centrifugation of treated-RRBC with different MMS were analyzed by 5–20% (w/v) gradient SDS-PAGE. Proteins were stained with Coomassie blue R-250 [39].

2.4. Hemolysis curve

The hemolysis curve of erythrocytes treated with different concentrations of MSS was obtained by measuring hemoglobin content in the supernatant. Absorbance at 412 nm of supernatant was measured in a Shimadzu, UV- Spectrophotometer, UV-1800. Data was normalized to hemoglobin content in samples treated with 100 μM MMS.

2.5. Changes in membrane properties using 2-photon excitation microscopy

The Laurdan molecule possesses a *dipole moment* (due to the partial charge separation at the naphthalene head) at the ground state. This dipole moment increases after excitation and the reorganization of the solvent molecules around the Laurdan molecule is responsible for the shift of the emission spectra towards longer wavelengths. In lipid bilayer, Laurdan is used to detect membrane heterogeneity since its emission spectrum depends on the phase state of the bilayer: the spectrum presents a maximum at 440 nm when the phospholipids are in gel phase and a maximum at 490 nm when they are in liquid/fluid phase. The naphthalene moiety of Laurdan locates in the membrane at the level of the glycerol backbone of the phospholipids and the shift of the emission spectrum

has been attributed to dipolar relaxation, involving the few water molecules present in the bilayer at this level [40]. Generalized polarization (GP) is a method used to quantify the spectral shift. Its value is determined by Eq. (1) [40,41], where I_{440} and I_{490} correspond to the emission intensities at 440 and 490 nm, respectively.

$$GP = (I_{440} - I_{490})/(I_{440} + I_{490}) \quad (1)$$

Parassasi et al. measured time-resolved emission spectra and they observed that molecules with emission centered at 440 nm have a shorter lifetime value than molecules emitting at 490 nm. The bathochromic shift of the emission spectrum is due to two effects; the polarity of the environment (ground state of the fluorophore) and the rate of dipolar relaxation of molecules or molecular residues that can reorient around Laurdan's fluorescent (naphthalene) moiety during its excited-state lifetime [40,42,43]. In biological membranes, these effects are related to the content (polarity) and molecular dynamics (mobility) of the water molecules around the Laurdan dipole. These two effects can be discriminated using lifetime measurements of Laurdan at the two extreme wavelengths of its emission spectra [43–45].

2.6. The phasor FLIM method

The phasor analysis is a frequency domain representation of the fluorescence lifetime measured at a single frequency. The phasor analysis approach is based on the transformation of the fluorescence decay histogram I (t) into its sine and cosine components and does not require fitting of the data to exponential decays [46]. Data are displayed in a polar plot (phasor plot) with coordinates $S = M \cos \phi$ and $G = M \sin \phi$, with ϕ being the phase delay and M the demodulation of the harmonic response to an excitation with sinusoidal modulated light [47,48]. For single exponential decays Equations 2–3 show the relation between lifetime and phase shift (Eq. (2)) and modulation (Eq. (3)), in the frequency domain.

$$\mathrm{Tan}\phi = \omega\tau_p \quad (2)$$

$$M = (1 + \omega^2\tau^2{}_m)^{-1/2} \quad (3)$$

Where ω is the angular frequency (equal to $2\pi f$, where f is the modulation frequency), τ_p and τ_m correspond to the lifetime phase and modulation respectively. In the phasor representation, a point (phasor), with particular S and G coordinates, represents each fluorescent species or excited state involved, independently of the number of exponentials needed to describe its decay. In an image, the lifetime will be determined at each pixel and its corresponding phasor will be located on the phasor plot. Thus, the phasor plot contains as many phasors as the number of pixels acquired in the image. The phasor analysis does not require accurate determination of the underlying lifetime components, the location and the relationship between the phasors will give information about the system [46]. The phasor plot approach has been used in several different applications; for example, ion concentration determination [49,50], protein conformation in vitro [51] and quantitative biology [52], among others.

2.7. The spectral phasor method [36,37]

In the spectral image, each pixel contains the emission spectrum at that pixel. Therefore, an emission curve is associated with every pixel. The spectral image can be analyzed in a global manner using the phasor approach where the Fourier sine and cosine transforms of a given spectrum are calculated (meaning at each pixel of the spectral image). In this transformation, two coordinates are calculated G and S. G correspond to the cosine transform (x coordinate in a polar plot) and S corresponds to the sine transform (y coordinate in a polar plot). The G and S component are calculated using the following mathematical expressions:

$$X = G = \frac{\sum_\lambda I(\lambda)\cos(2\pi n\lambda/L)}{\sum_\lambda I(\lambda)} \quad (4)$$

$$Y = S = \frac{\sum_\lambda I(\lambda)\sin(2\pi n\lambda/L)}{\sum_\lambda I(\lambda)} \quad (5)$$

Where L is the total wavelength range, $I(\lambda)$ corresponds to the intensity at a given wavelength and given pixel, and n is the harmonic order. A point at coordinates (g, s) is called a phasor and is represented in a polar plot. G and S take values between 1 to −1. The angular position in the polar plot (the phasor angle) is proportional to the spectral center of mass. The distance from the origin (the phasor radius) is inversely proportional to the spectral width. The Fourier space, i.e. the spectral phasor plot, has the properties of sum, difference, etc, providing the opportunity to judge the contributions from the different species, and the interactions between them, in a straightforward manner. These Fourier transformations allow us to determine, with a simple visual inspection, the presence of complex interactions in the Laurdan/membrane system without the assumption of a particular model.

The spectral phasor approach was first introduced by Fereidouni et al., for the blind unmixing of up to three different probe emissions in the same sample [37,53] and lately it has been used for both cuvette [37] and cell [54] analysis.

2.8. Data acquisition

Lifetime and intensity images were acquired in a two-photon microscope coupled with a FLIM box (ISS, Champaign IL). A Ti:Sapphire laser (Spectra-Physics Mai Tai) with 80 MHz repetition rate and tuned at 780 nm was used to excite the sample. A quarter wave-plate (CVI Laser Corp., Albuquerque, NM) was placed in the path of the beam before the light entered the microscope to minimize the polarization effects of the excitation light. The laser was coupled to a Olympus Fluoview FV 1000 microscope having a Olympus UPlanSApo 60x/1.20 W water immersion objective. The fluorescence signal was split in two using a Chroma Technology 470DCXR-BS dichroic beam splitter in the emission path and filters of 440/60 nm and 500/60 nm (Semrock, Rochester, NY. USA) were located in the detectors. Data were acquired by the SimFCS software developed at the Laboratory for Fluorescence Dynamics (www.lfd.uci.edu). Calibration of the system for intensity measurements was performed by measuring Laurdan in DMSO [55]. For lifetime measurements POPOP in ethanol which has a well-known single-exponential lifetime of ~1.35 ns [56] was used as a reference.

Spectral images were obtained in a Zeiss 710NLO microscope equipped with a spectral detector of 32 channels. A Ti:Sapphire laser (Spectra-Physics Mai Tai) with 80 MHz repetition rate and tuned at 780 nm was used to excite the sample.

2.9. Data analysis

GP images were obtained by applying the GP formula (Eq. (1)) using the images obtained with the emission filters 440/60 nm and 500/60 nm. The pixels corresponding to the plasma membrane were analyzed and the average GP value from the pixel histogram was obtained by fitting to a Gaussian distribution, this value is reported as GP_{avg}. Several images, (minimum 8, maximum 10), were processed in this manner to obtain the GP_{avg} [21,57] for the membrane of the erythrocytes incubated with different detergent concentrations. Image J software was used for this type of analysis.

FLIM images were obtained using the filters at 440/60 nm and 500/60 nm and transformed to the phasor coordinates using the SimFCS software (Laboratory for Fluorescence Dynamics Irvine, CA,

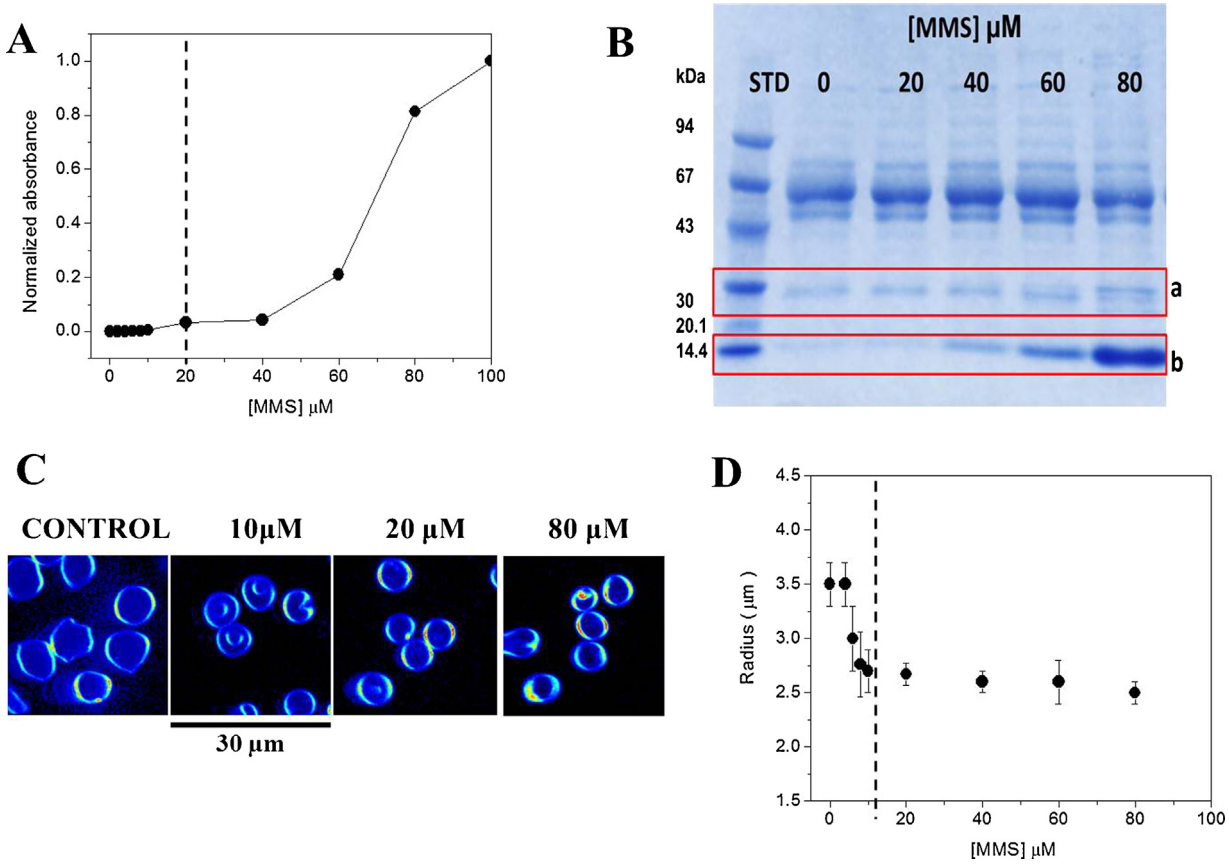

Fig. 1. RRBC treated with increasing concentrations of MMS. RRBC were incubated for 1 h at 37 °C with MMS concentration between 0.2–80 µM. [A] Hemoglobin in the incubation media, normalized absorbance at 412 nm. Vertical dashed line shows MMS concentration of 20 µM. [B] 5–20% SDS-PAGE of the supernatant of the samples treated with different MMS concentrations. Rectangles labeled *a* and *b* indicate the protein bands of 30 and 14 kDa, respectively.[C] Representative Laurdan intensity images of erythrocytes treated with increasing concentrations of MMS.[D] Changes in the radius (µm) of RRBC treated with increasing MMS concentration determined from the images in C using Image J software.

USA) as described in previously published papers [46]. In brief, the fluorescence decay in each pixel of the FLIM image was transformed into the sine and cosine components, which were then represented in a 2D polar plot (phasor plot), according to the equations previously defined [46]. SimFCS software used in reciprocal mode enables each point of the phasor plot to be mapped to each pixel of the FLIM image.

Spectral images were Fourier transformed (using the first harmonic) to the phasor coordinates using the SimFCS software (Laboratory for Fluorescence Dynamics Irvine, CA, USA) as described in previously [36,37]. The length of the spectrum (L) used for the spectral images was 400–600 nm.

3. Results and discussion

3.1. Hemolysis curve of rabbit erythrocytes (RRBC) treated with MMS

RRBC were incubated with MMS in a concentration range from 0.2 to 1000 µM. Hemolysis curve (Fig. 1A) shows a 50% hemolysis at 70 µM MMS. Protein released to the incubation media was analyzed using a 5–20% SDS-PAGE (Fig. 1B). Protein profile is the same for control and treated sample with 20 µM MMS; instead at higher MMS concentration (40–80 µM) an increase in proteins bands corresponding to 30 and 14 kDa is observed (Fig. 1B lines a and b). Protein band of ~14 kDa (box b) corresponds to hemoglobin (also detected at 415 nm in Fig. 1A). Protein band of ~30 kDa (box a) may correspond to aquaporin-1 and glyceraldehyde 3-P dehydrogenase; however, it was not the interest of this report to accurately identify these proteins, but instead to determine if protein was released to explain changes in the membrane properties.

The morphological changes of RRBC treated with 80 uM of MMS can be observed in the video S1 (supplementary material). Within the first minute, MMS induces crenation of the RRBC because of cell shrinkage, followed by a gradual volume increase and finally lysis of the cells.

Laurdan intensity images (Fig. 1C) for control erythrocytes (zero MMS) show concave discoid erythrocytes and echinocytes. As the concentration of MMS increases the size of the erythrocytes decreased reaching a plateau around 20 µM MMS (Fig. 1D). The total decrease in size observed was approximately 34% from the original size.

3.2. Effect of MMS on membrane fluidity of RRBC

Laurdan Generalized Polarization Imaging studied the average changes in membrane fluidity of the RRBC during their interaction with MMS. Laurdan GP images (Fig. 2A) were obtained after incubation of erythrocytes with MMS for 1 h at 37 °C. The average GP value for the membrane (calculated from the membrane pixel histogram of ten images for each MMS concentration) is shown. No changes in the average GP value (0.32 +/− 0.01) for the membrane were observed in the concentration range tested (Fig. 2B). The absence of changes in the average GP while the radius of the erythrocyte decreased by 34% could be explained either by an homogeneous removal of material from the membrane (with no preference of any particular lipid domain) or by small changes veiled by the averaging nature of this particular analysis.

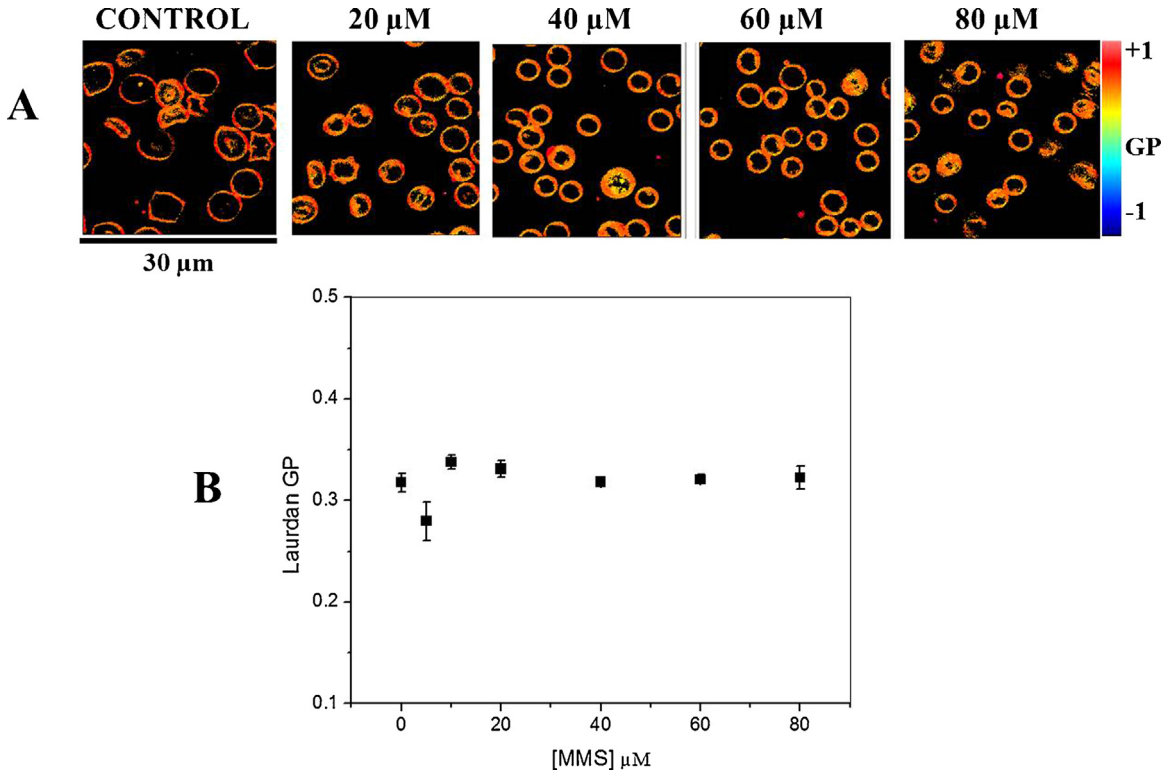

Fig. 2. Laurdan Generalized Polarization (GP) imaging for the MMS-erythrocytes interaction. [A] GP images of RRBC recovered in the pellet after incubation (hematocrit 5% v/v) with increasing concentrations of MMS. Hematocrit for the imaging was 0,2% v/v. [B] Average GP value obtained from the GP image histogram. For all the intensity analysis, 10 images for each MMS concentration were analyzed. Measurements performed at 37 °C.

3.3. *Laurdan FLIM phasor analysis*

Laurdan lifetime was measured in order to obtain more information about the changes in the membrane of RRBC induced by MMS incorporation. Data is presented in two parts; erythrocytes treated with sublytic concentration of MMS (0–10 µM) (Fig. 3) and erythrocytes treated with lytic concentration of MMS (20–80 µM) (Fig. 4). FLIM data were taken at 440 and 500 nm but both Figures shows the analysis obtained at 440 nm since similar conclusions are obtained at 500 nm. The FLIM data were Fourier transformed into the phasor representation, and analysis was performed using SimFCS software (methods). Fig. 3A shows the FLIM-phasor plot for RRBC control and incubated with MMS at sublytic concentrations (4–10 µM). A cluster of phasors located at *G* and *S* values around 0.5 is observed for control and treated RRBC. Using SimFCS software, three square-cursors (red, green and blue) were used to map each point at the phasor plot (Fig. 3A) to each pixel of the intensity image (Fig. 3B) to obtain a pseudo colored image (Fig. 3C) where the origin of each phasor is shown. Thus, red areas in Fig. 3C indicate areas where Laurdan has a shorter lifetime as compared with the green and blue areas, being the blue pixels the ones with the longer lifetime for the probe. The percentage of green (65%) and red pixels (35%) corresponding to long and short lifetimes respectively, remained similar until 4 µM MMS (Fig. 3D). At higher MMS concentration, a slight decrease in red pixels (and a slight increase in green pixels) percentage is observed, although this difference is not significant. Few blue pixels are observed at this MMS concentration range. These data indicate the existence of membrane heterogeneity in terms of polarity (water content) in intact and treated-erythrocytes with sublytic concentrations of MMS.

Fig. 4 shows the FLIM phasor analysis for control and treated erythrocytes with hemolytic concentrations of MMS (20–80 µM). Same red, green and blue cursors used in Fig. 3 are used for the analysis at lytic condition. As the concentration of MMS increases, the cluster of phasors (Fig. 4A) move towards longer lifetimes (to the left of the universal semi-circle) with respect to the control At 80 µM of MMS the cluster of phasors locates inside the blue cursor (long lifetimes). Fig. 4C shows clearly the increment of pixels corresponding to blue cursor (long lifetimes) and practically the disappearance of pixels corresponding to red cursor (short lifetimes) in erythrocytes membrane treated with 80 µM of MMS. The cluster from channel 500 nm (data not showed) exhibit a similar behavior, with movement to longer lifetimes and a final position outside the semi-circle, indicative of a dipolar relaxation processes [43,58,59].

The short Laurdan lifetime in control erythrocyte might be due to a quenching effect suppressed as the concentration of MMS increases. In this context, two are the possible scenarios: (a) In control erythrocytes, Laurdan is being quenched by water molecules present at the membrane interphase, and the insertion of MMS molecules diminish this quenching effect by displacing the water molecules. Quenching of Laurdan by water molecules is a well reported observation[43] [40]. (b) In control erythrocytes, the hemoglobin inside the erythrocyte is quenching Laurdan and as MMS increase and hemoglobin is released from the cell, the quenching effect diminishes. Hemoglobin content inside erythrocytes is around 20 mM and the molecules near the inner membrane surface would be the responsible for the quenching of fluorescent dyes [60]. There are not specific reports (to the best of our knowledge) on quenching of Laurdan by hemoglobin, however it is well reported the quenching effect for fluorescent probes such as 1,6-diphenyl-l,3,5-hexatriene (DPH) [61], 12-(9-anthroyl)stearic acid (AS) [62] and n-(9-anthroyloxy)-stearic and palmitic acids (n-AS and n-AP) and 9-vinyl anthracene [60].

In the literature, authors acknowledge the possible quenching of Laurdan by hemoglobin, but they bypass the problem by

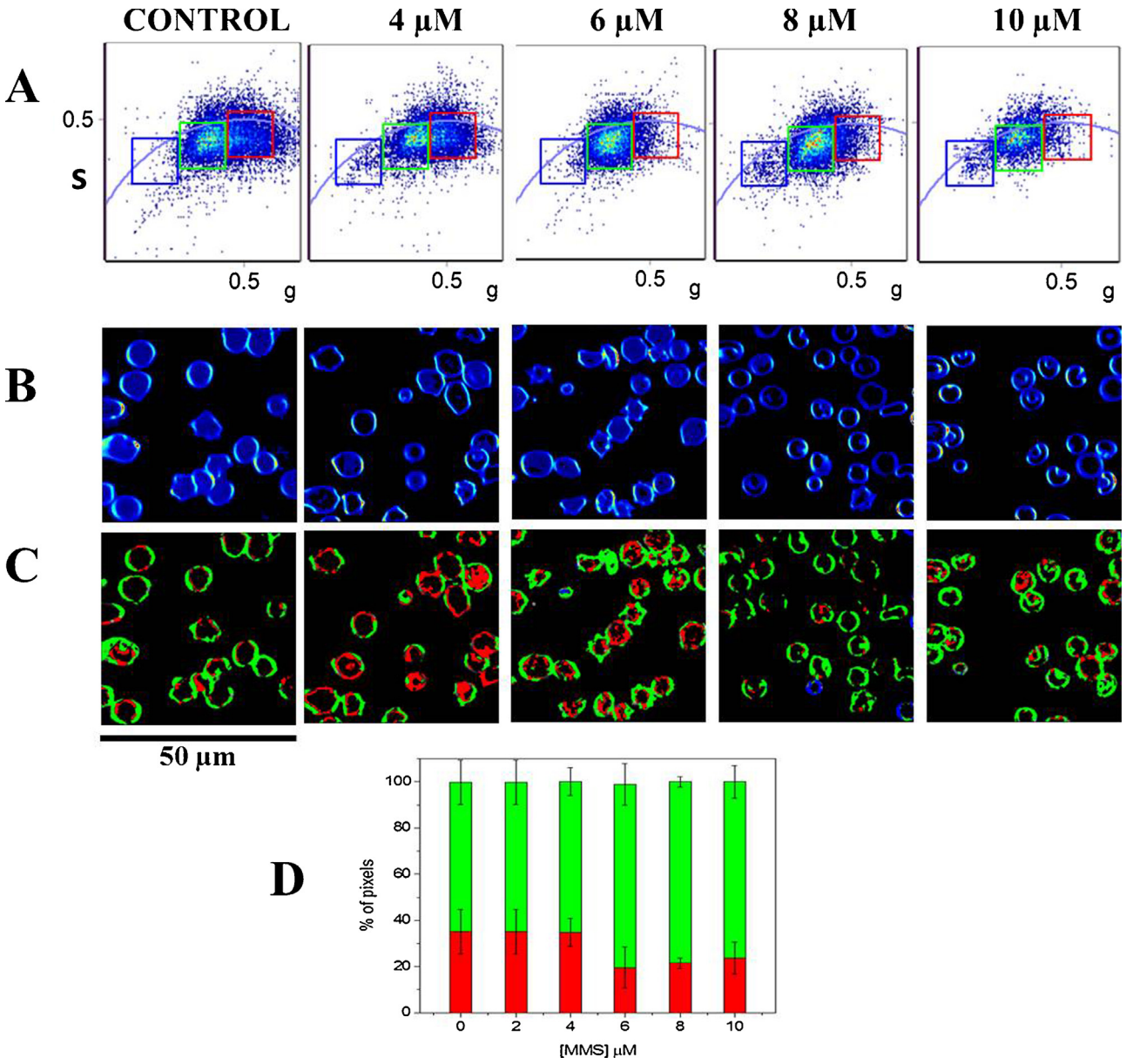

Fig. 3. Laurdan FLIM-phasor analysis for sublytic concentration of MMS. [A] Phasor plot for RRBC incubated with different MMS concentrations. Three cursors were used for the analysis red (short lifetimes), green (middle lifetimes) and blue (long lifetimes) [B] Laurdan intensity images. [C] Intensity image pseudo-colored according the cursors in A mapping each point at the phasor plot to each pixel of the intensity image B. [D] Number of pixels included in the red and green cursor as MMS concentration increase. Lifetime data were taken using 2-photon excitation at 780 nm and emission at 440 nm. SimFCS software was used for the analysis. Measurements performed at 37 °C. (For interpretation of the references to colour in this figure legend, the reader is referred to the web version of this article.)

either working at the same hematocrit so hemoglobin concentration would be constant [63], applying a correction factor for the energy transfer [61] or working with hemoglobin depleted erythrocytes (ghosts) [64]. In the this work we explored the possible quenching of Laurdan by hemoglobin

3.4. Quenching of laurdan by hemoglobin

In order to distinguish if the quenching effect is due to hemoglobin or MMS, ghost erythrocytes were obtained by hypotonic lysis solution of PBS. With this protocol, we obtained closed hemoglobin depleted erythrocytes (Fig. 5B control) similar to the ones obtained by 80 µM MMS treatment (Fig. 5A, 80 µM). Ghost were incubated with two concentrations of MMS; 10 µM, concentration where neither changes in Laurdan lifetime (Fig. 3) nor hemoglobin release (Fig. 1) was observed and 80 µM where large Laurdan lifetime changes (Fig. 4) and hemoglobin released was observed (Fig. 1).

FLIM data for erythrocytes and ghosts were obtained under the same buffer and temperature conditions. Analysis was performed using the same color (red, green and blue) and location of the cursors used in Fig. 3 and 4. For erythrocytes incubated with 10 and 80 µM MMS (Fig. 5A), FLIM phasor analysis shows the movement of the phasor cluster toward longer lifetimes with respect to control. For the ghost samples, the cluster of phasor is in the blue location independently of the MMS concentration used. These experiments clearly show that the changes in Laurdan lifetime as the concentration of MMS increased are mainly due to the decrease of hemoglobin content inside the erythrocyte (by the effect of the detergent).

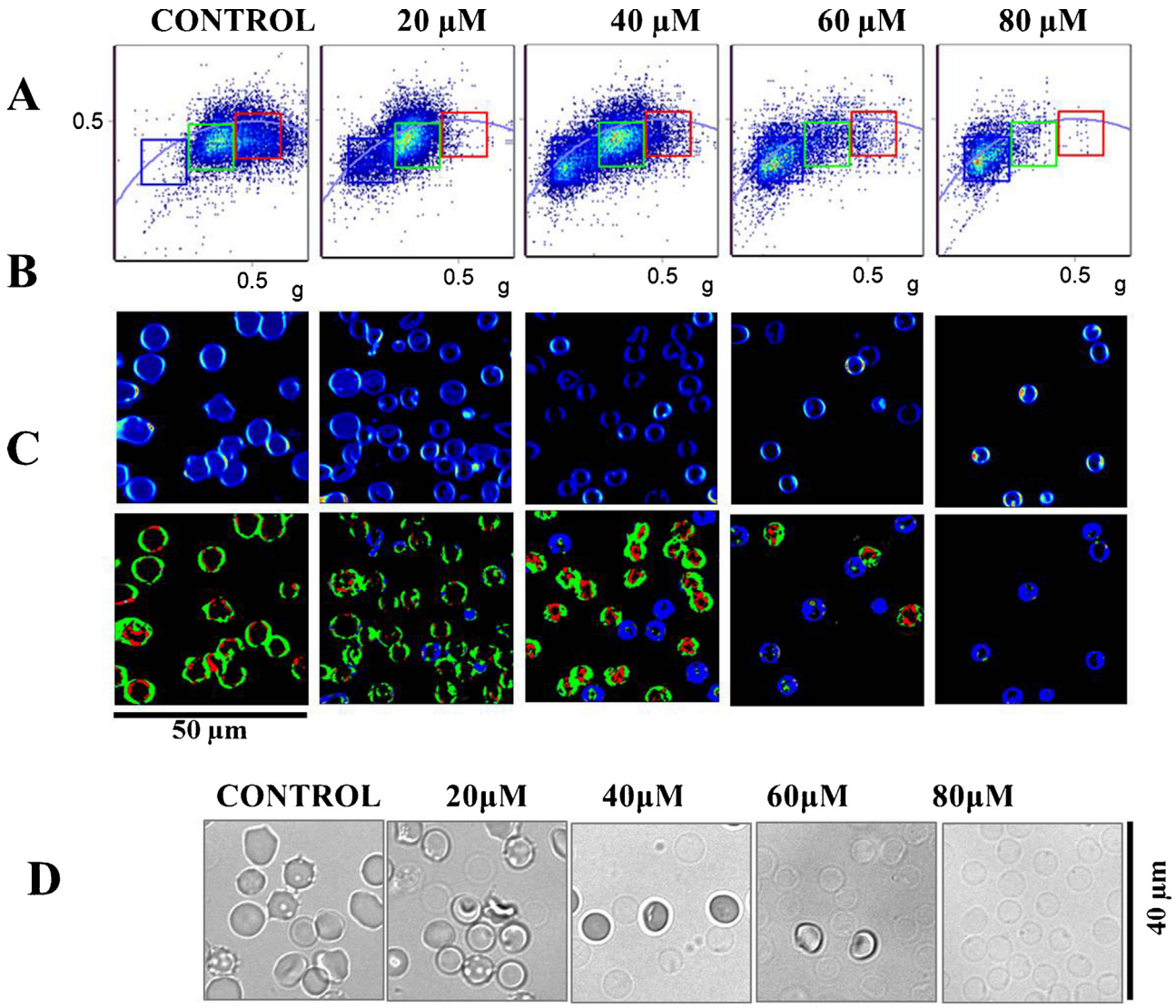

Fig. 4. Laurdan FLIM-phasor analyses for lytic concentration of MMS. [A] Phasor plot for RRBCs incubated with MMS concentrations from 20 to 80 µM. Cursors red, green and blue have the same location used in Fig. 3. [B] Laurdan intensity images. [C] Intensity image pseudo-colored according the cursors in A, mapping each point at the phasor plot to each pixel of the intensity image B. [D] Light microscopy images of RRBC treated with MMS at different concentrations. Image size 40 × 40 µm Lifetime data were taken using 2-photon excitation at 780 nm and emission at 440 nm. SimFCS software was used for the analysis. Measurements performed at 37 °C. (For interpretation of the references to colour in this figure legend, the reader is referred to the web version of this article.)

3.5. *Changes in membrane fluidity detected in the presence of hemoglobin*

Results in Fig. 5 show that FLIM measurements depend on the quenching by hemoglobin; therefore they cannot be used to study the effect of MMS on the fluidity of the erythrocytes, Recently, Malacrida et al. [37] reported the spectral analysis for Laurdan (a model-free, rapid and reliable method) to study membrane heterogeneity. We explored this methodology aiming to be able to observe changes in the membrane fluidity in the presence of hemoglobin using Laurdan as fluorescent probe.

Spectral images were taken for control and MMS treated RRBC and two type of analysis were performed, the spectral phasor analysis (Fig. 6, ABC and abc) and the traditional average emission spectra from the whole image (Fig. 6 D and d). Fig. 6 shows the two types of analysis for control (upper panel) and MMS treated erythrocytes (lower panel). Analysis for each condition considered three images of Laurdan labeled RRBC (L) and one image of unlabeled RRBC (Hb) which correspond to the signal from hemoglobin inside the erythrocyte.

The full spectral phasor plot for control (Fig. 6A) and treated with 80 µM MMS (Fig. 6a) show the cluster distribution located in the upper half of the phasor plot for the two cases. A zoom image of the full phasor plot for control (Fig. 6B) and MMS treated cells (Fig. 6b) show details of the phasor distribution. For the analysis, in Fig. 6(B and b) a red cursor was used to identify the phasors for unlabeled RRBC (image Hb) and two cursor (cyan and yellow) for the phasor from the Laurdan in the membrane (images L).

Visual comparison of Fig. 6B and b shows in control erythrocytes (Fig. 6B) a population of phasors inexistent in the MMS treated erythrocytes (Fig. 6b) connecting the hemoglobin (red) to the Laurdan cluster (cyan/yellow). This population corresponds to phasors from pixels having contribution of hemoglobin and Laurdan not present in the MMS treated cells where hemoglobin is depleted. To consider this population in the analysis, a linear combination of red/yellow and red/cyan cursors (Fig. 6A, bottom/left corner) was used to map each point at the phasor plot to each pixel of the intensity image. Using this color scale, control erythrocytes (Fig. 6C, L) colored mainly with cyan at the membrane and yellow/red inside (indicating heterogeneity of hemoglobin content in the RRBC) and

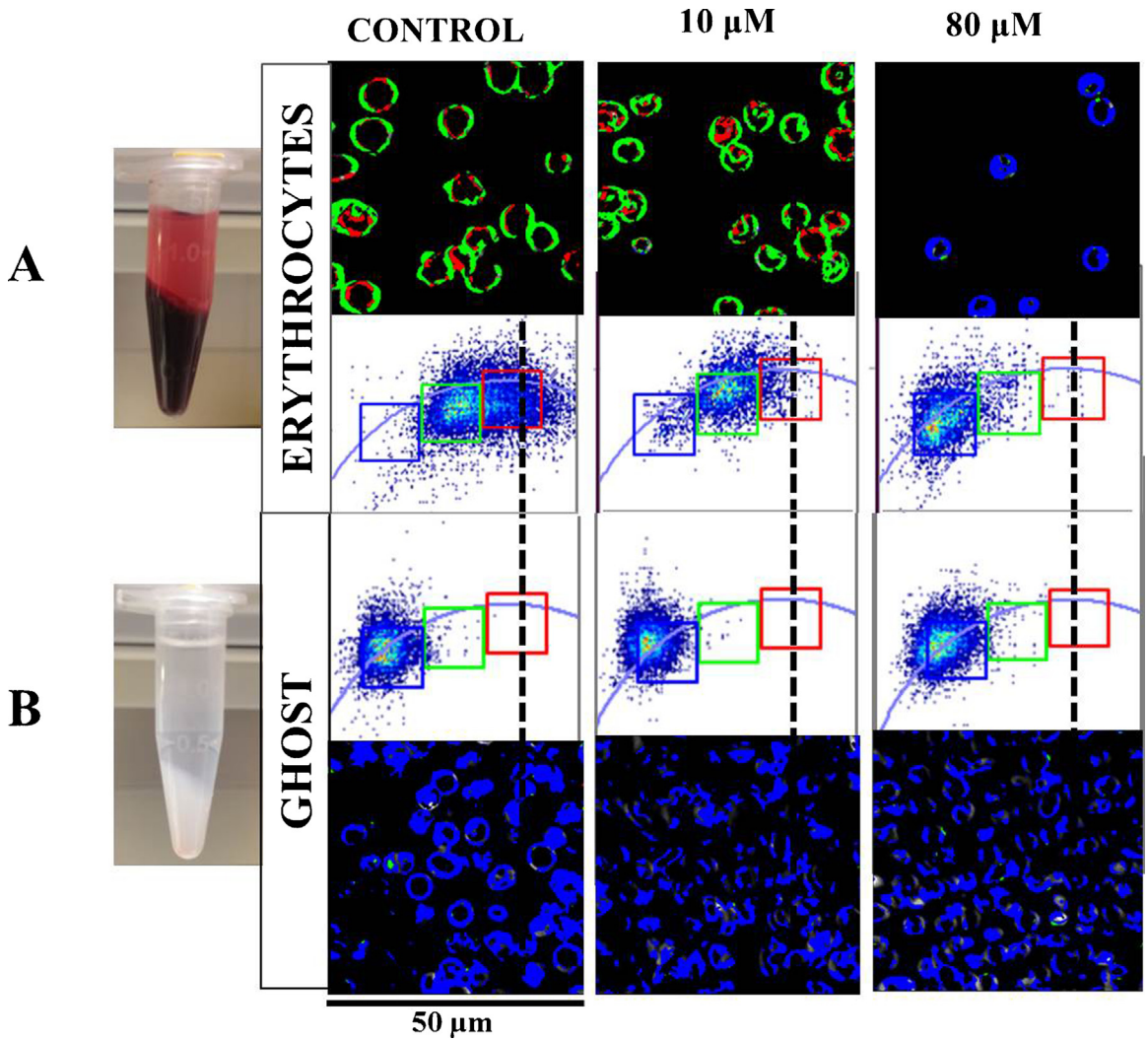

Fig. 5. FLIM phasor analysis for intact and ghosts RRBC. Under the same experimental conditions, erythrocytes and ghosts (prepared with hypotonic PBS) were incubated with 10 and 80 μM MMS for 1 h at 37 °C. For FLIM phasor analysis the red, green and blue cursors have the same location used in Figs. 3 and 4. Measurements performed at 37 °C. (For interpretation of the references to colour in this figure legend, the reader is referred to the web version of this article.)

MMS treated RRBC (Fig. 6c, L) colored mainly yellow and some cyan regions. Accordingly, Fig B and b, shows the displacement of the membrane phasors to longer wavelengths (from cyan to yellow) indicating that MMS is increasing the content of water at the interface, where Laurdan is located. It is important to highlight at this point, that the spectral phasor analysis allowed observing these displacements despite the presence of hemoglobin.

To appreciate the sensitivity of the spectral phasor analysis, the same spectral images were analyzed obtaining the full emission spectra. Fig. 6D and d show the emission spectra for hemoglobin (red) and control RRBC (cyan), and in Fig. 6d the emission spectra of 80 μM MM treated cells was also added (yellow). The cyan arrow in 6d shows the spectral displacement of laurdan spectra produced by the treatment with MMS (spectras cyan and yellow). This small spectral displacement could not be detected using GP analysis (Fig. 2). It is important to notice in Fig. 6d that the shape of the Laurdan spectra in control (cyan) and in 80 μM MMS treated cells (yellow) did not change.

Pixels cyan and yellow (Fig. C and c) correspond to areas in the membrane with different fluidity (domains with different water content) and the changes in the number and spatial distribution of these pixels indicate the changes in the membrane fluidity generated by the presence of the detergent. An increment of more fluid domains is observed in erythrocytes treated with 80 μM MMS.

4. Conclusion

4.1. The insertion of MMS into the bilayer

Changes in the erythrocyte membrane due to its interaction with MMS were followed using Laurdan as a fluorescent dye. We tried three experimental approaches in order to observe the changes in the membrane of erythrocytes in the presence of hemoglobin; GP, FLIM and spectral imaging. FLIM measurements analyzed using the phasor approach clearly showed the hemoglobin quenching effect on Laurdan and the increase in lifetimes as hemoglobin is released from the erythrocytes due to the interaction with the sucrose detergent MMS. Thus, the changes in Laurdan FLIM after interaction with MMS have a strong contribution from hemoglobin content. The spectral phasor approach allowed the analysis of the Laurdan signal in the membrane of erythrocytes in the presence of hemoglobin, and our results showed an increase in water content at the membrane interface after insertion of the MMS molecules. Spectral phasor analysis relays on the shape the spectra (wavelength at the emission maxima and width at the middle high), and in these studies, despite the changes in lifetime, no changes in the shape of the Laurdan emission spectra were observed.

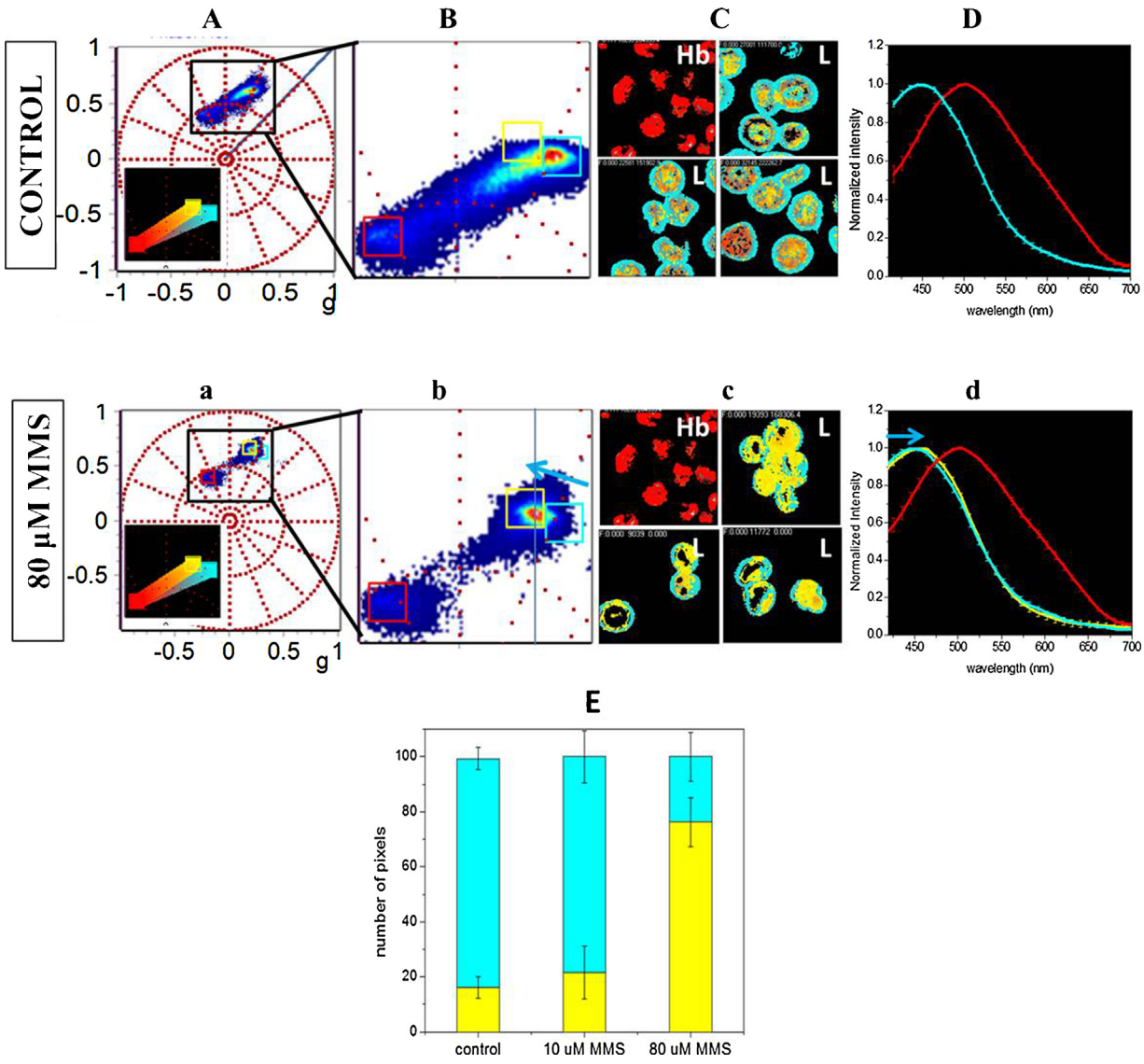

Fig. 6. Spectral phasor analysis. [A,a] Full spectral phasor representation of spectral images from unlabeled and Laurdan labeled erythrocytes. Square colored cursors used in the analysis: red for unlabeled RRBC and cyan/yellow for Laurdan labeled RRBC. At the bottom left of panels A and a it is shown the linear combination of colors used for the analysis, red-yellow and red-cyan. [B,b] Zoom image of the spectral phasor in A,a. **[C, c]** Intensity image pseudo-colored according to the linked colored cursor in the phasor plot shown in A, a. Hb indicate erythrocytes without labeling used to record the signal of hemoglobin, L indicate Laurdan labeled erythrocytes. [D, d] Emission spectra obtained from the full spectral images used to create spectral phasor in A,a. Emission spectra for RRBC unlabeled (red), Laurdan labeled control (Cyan) and Laurdan labeled treated with 80 μM MMS. [E] Number of pixels (cyan and yellow) from Laurdan labeled RRBC (L images in C, c). Measurements performed at 37 °C. (For interpretation of the references to colour in this figure legend, the reader is referred to the web version of this article.)

Fig. 7A shows a cartoon representation to explain the results on the insertion of MMS into the RRBC membrane. The bulkiness of the sucrose head present in MMS would allow water molecules to enter into the interface.

4.2. The solubilization process of RRBC with MMS

According to our data, the solubilization of erythrocytes by MMS can be separated in two regions, before (<20 μM MMS) and after hemolysis (>20 μM MMS).

Pre-hemolysis (MMS <20 μM) (Fig. 7B): MMS is a micelle forming detergent cmc = 19 μM [65] and at this concentration range, it will interact with the membrane forming micelles and removing material from it. Our data show changes in the size of the erythrocytes with no changes in the membrane properties, indicating a homogeneous removal of mainly lipids (PAGE gel does not show changes in protein content). There is also no evidence of preferential removal from areas of different fluidity (FLIM pixel analysis Fig. 3D). This homogeneous removal of lipids independent of the phase state was previously reported for MMS interacting with POPC and POPC cholesterol GUVs where decrease in volume was also observed [66].

Hemolysis (MMS >20 μM until 80 μM) (Fig. 7B): in this concentration range, the size of the erythrocyte does not change, but hemoglobin is released leaving the empty whole ghost (Fig. 4E). No further studies were performed on the hemoglobin releasing mechanism. On the other hand, the changes observed in the lifetime data at this condition, were mainly due to the release of hemoglobin. The decrease in hemoglobin content diminishes the quenching effect on Laurdan (Fig. 4A). Spectral phasor analysis could successfully discriminate Laurdan signal at the membrane in the presence of hemoglobin and the analysis shows that insertion of the MMS in the bilayer produces an increase in water accessibility in the membrane, inducing an increase in membrane fluidity.

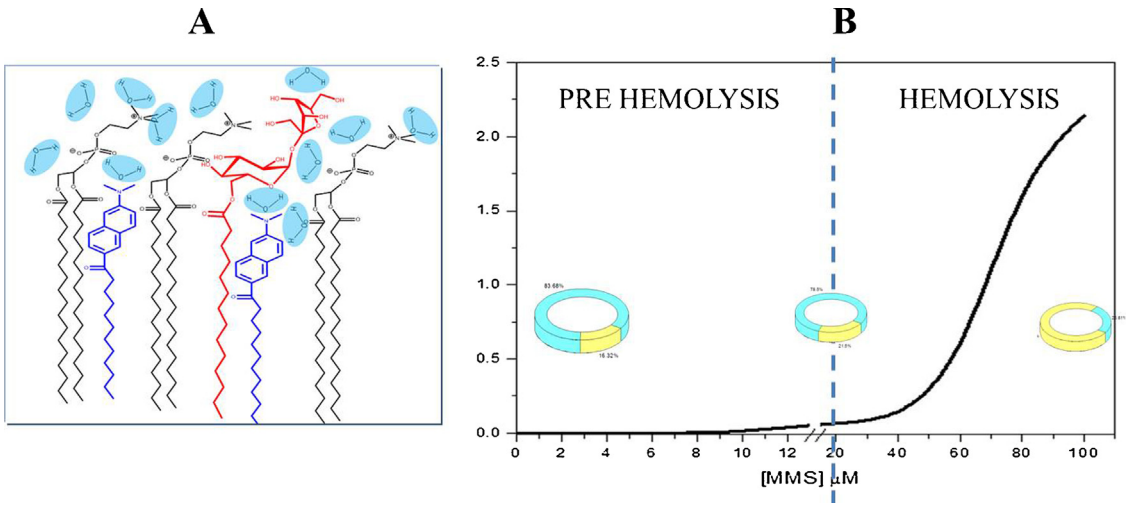

Fig. 7. Diagram for the interaction of RRBC and MMS.

Acknowledgements

Financial support: Fondecyt#1140454 (S.S.), Fondecyt #1080412 (G.G.) and Beca de Doctorado Conicyt (C.S.). Agencia Nacional de Promoción Científica y Tecnológica (PICT 2657/2013) (VH). Ministerio de Economiía y Competitividad# FIS2015-70339-C2-2-R (M.P.L.). Some experiments reported in this publication were performed at the Laboratory for Fluorescence Dynamics (LFD) at the University of California, Irvine (UCI). The LFD is supported jointly by the National Institute of General Medical Sciences of the National Institutes of Health (8P41GM103540), and UCI. The authors wish to thank Dr. Kerry M. Hanson, University of California, Riverside, for manuscript feedback and Dr. Leonel Malacrida (LFD) for analysis support.

Appendix A. Supplementary data

Supplementary data associated with this article can be found, in the online version, at https://doi.org/10.1016/j.colsurfb.2017.10.068.

References

[1] U. Kragh-Hansen, M. leMaire, J.V. Möller, The mechanism of detergent solubilization of liposomes and protein-containing membranes, Biophys. J. 75 (1998) 2932–2946.
[2] C. Toro, et al., Solubilization of lipid bilayers by myristyl sucrose ester: effect of cholesterol and phospholipid head group size, Chem. Phys. Lipids 157 (2009) 104–112.
[3] T. Yakushi, M. Kojima, K. Homma, Isolation of vibrio alginolyticus sodiumdriven flagellar motor complex composed PomA and PomB solubilized by sucrose monocaprate, Microbiology-Sgm 150 (2004) 911–920.
[4] H. Heerklotz, Interactions of surfactants with lipid membranes, Q. Rev. Biophys. 41 (2008) 205–264.
[5] D. Lichtenberg, et al., Detergent solubilization of lipidbilayers: a balance of driving forces, Trends Biochem. Sci. 38 (2013) 85–93.
[6] N. Becerra, et al., Solubilization of dodac small unilamellar vesicles by sucrose esters – A fluorescence study, Colloids Surf. A 272 (2006) 2–7.
[7] F.J. Cuevas, D.M. Jameson, C.P. Sotomayor, Modulation of reconstituted pig kidney Na+/K+-ATPase activity by cholesterol in endogenous lipids vesicles: role of lipid domains, Biochemistry 45 (2006) 13855–13868.
[8] K. Jacobson, O.G. Mouritsen, R.G.W. Anderson, Lipid rafts: at a crossroad between cell biology and physics, Nat. Cell Biol. 9 (2007) 7–14.
[9] K. Simons, E. Ikonen, Functional rafts in cell membranes, Nature 387 (1997) 569–572.
[10] A. Tsamaloukas, H. Szadkowska, H. Heerklotz, Nonideal mixing in multicomponent lipid/detergent systems, J. Phys. Condens. Matter 18 (28) (2006) S1125–1138.
[11] H. Heerklotz, Triton promotes domain formation in lipid raft mixtures, Biophys. J. 83 (5) (2002) 2693–2701.
[12] D. Lichtenberg, F.M. Goñi, H. Heerklotz, Detergents-resistant membranes should not be identified with membrane rafts, Trends Biochem. Sci. 30 (2005) 430–436.
[13] L.J. Pike, Rafts defined: a report on the Keystone symposium on lipid rafts and cell function, J. Lipid Res. 47 (2006) 1597–1598.
[14] H. Ahyayauch, R.M. Alonso A, M. Bennouna, F.M. Goñi, Surfactant effects of chlorpromazine and imipramine on lipid bilayers containing sphingomyelin and cholesterol, J. Colloid Interface Sci. 256 (2) (2002) 284–289.
[15] J. Ruiz, G.F. Alonso, A surfactant-induced release of liposomal contents. A survey of methods and results, Biochim. Biophys. Acta. 937 (1) (1988) 127–134.
[16] A. Ciana, et al., On the association of lipid rafts to the spectrin skeleton in human erythrocytes, Biochim. Biophys. Acta 1808 (2011) 183–190.
[17] S.A. Sánchez, M.A. Tricerri, G.E, Laurdan GP fluctuations measures membrane packing micro heterogeneity in vivo, Proc. Natl. Acad. Sci. U. S. A. 109 (19) (2012) 7314–7319.
[18] B.R. Casadei, et al., Brij detergents revealvnew aspects of membrane microdomain in erythrocytes, Mol. Membr. Biol. 31 (6) (2014) 195–205.
[19] A. Ciana, C. Achilli, G. Minetti, Membrane rafts of the human red blood cell, Mol. Membr. Biol. 31 (2) (2014) 47–57.
[20] B.M. Stott, et al., Use of fluorescence to determine the effects of cholesterol on lipid behavior in sphingomyelin liposomes and erythrocyte membranes, J. Lipid Res. 49 (6) (2008) 1202–1215.
[21] S.A. Sánchez, et al., Lipid packing determines protein-membrane interactions: challenges for apolipoprotein A-I and high dDensity lipoproteins, Biochim. Biophys. Acta 1798 (7) (2010) 1399–1408.
[22] C.P. Sotomayor, et al., Modulation of pig kidney Na+/K+-ATPase activity by cholesterol: role of hydration, Biochemistry 39 (35) (2000) 10928–10935.
[23] P.S.C. Preté, et al., Multiple stages of detergent-erythrocyte membrane interaction—A spin label study, Biochim. Biophys. Acta 1808 (2011) 164–170.
[24] F.M. Goñi, et al., The interaction of phosphatidylcholine bilayers with Triton X-100, Eur. J. Biochem. 160 (3) (1986) 659–665.
[25] P.S.C. Preté, et al., Quantitative assessment of human erythrocyte membrane solubilization by Triton X-100, Biophys. Chem. 97 (2002) 1–5.
[26] D. Lichtenberg, Characterization of the solubilization of lipid bilayers by surfactants, Biochim. Biophys. Acta 821 (1985) 470–478.
[27] D. Lichtenberg, E. Opatowski, M.M. Kozlov, Phase boundaries in mixtures of membrane-forming amphiphiles and micelle-forming amphiphiles, Biochim. Biophys. Acta 1508 (2000) 1–19.
[28] S.V.P. Malheiros, E. de Paula, N.C. Meirelles, Contribution of trifluoperazineylipid ratio and drug ionization to hemolysis, Biochim. Biophys. Acta 1373 (1998) 332–340.
[29] H. Noritomi, et al., Forward and backward extractions of cytochrome c using reverse micellar system of sucrose fatty acid ester, Colloid Polym. Sci. 284 (2006) 604–610.
[30] H. Noritomi, et al., Application of sucrose fatty acid ester to reverse micellar extraction of lysozyme, Colloid Polym. Sci. 284 (2006) 677–682.
[31] H. Noritomi, et al., How can temperature affect reverse micellar extraction using sucrose fatty acid ester? Colloid Polym. Sci. 284 (2006) 683–687.
[32] M.F. Henning, S.A. Sánchez, L. Bakás, Visualization and analysis of lipopolysaccharide distribution in binary phospholipid bilayers, Biochem. Biophys. Res. Commun. 383 (2009) 22–26.
[33] S.A. Sanchez, et al., Methyl-β-cyclodextrins preferentially remove cholesterol from the liquid disordered phase in giant unilamellar vesicles, J. Membr. Biol. 24 (1) (2011) 1–10.
[34] S.A. Sánchez, et al., Laurdan Generalized Polarization: from cuvette to microscope, in: A. Mendez-Vilas, Diaz (Eds.), Modern Research and

Educational Topics in Microscopy. Applications in Physical/Chemical Sciences, 2007, pp. 1007–1014.
[35] M.A. Digman, et al., The phasor approach to fluorescence lifetime imaging analysis, Biophys. J. 94 (2) (2008) L14–L16.
[36] O. Golfetto, H.E, E. Gratton, The Laurdan spectral phasor method to explore membrane micro-heterogeneity and lipid domains in live cells, in: D.M. Owen (Ed.), Methods in Membrane Lipids. Methods in Molecular Biology, 1232, Springer New York, 2014, pp. 273–290.
[37] L. Malacrida, G.E, D.M. Jameson, Model-free methods to study membrane environmental probes: a comparison of the spectral phasor and generalized polarization approaches, Methods Appl. Fluoresc. 3 (4) (2015) 047001.
[38] I.R. Vlahov, P.I. Vlahova, R.J. Lindhart, Regioselective synthesis of sucrose monoesters as surfactants, J. Carbohyd. Chem. 16 (1997) 1–10.
[39] F.C. Velásquez, M.S. Bakás L, V. Herlax, Induction of eryptosis by low concentrations of E: coli alpha-hemolysin, Biochim. Biophys. Acta 1848 (2015) 2779–2788.
[40] T. Parasassi, et al., Laurdan and prodan as polarity-sensitive fluorescent membrane probes, J. Fluorescence 8 (4) (1998) 365–373.
[41] T.S. Parasassi, et al., Quantitation of lipid phases in phospholipid vesicles by the generalized polarization of laurdan fluorescence, Biophys. J. 60 (1991) 179–189.
[42] M. Viard, et al., Origin of laurdan sensitivity to the vesicle-to-micelle transition of phospholipid-octylglucoside system: a time-resolved fluorescence study, Biophys. J. 80 (2001) 347–359.
[43] Ottavia Golfetto, E.H, Enrico Gratton, Laurdan fluorescence lifetime discriminates cholesterol content from changes in fluidity in living cell membranes, Biophys. J. 104 (6) (2013) 1238–1247.
[44] T. Parasassi, C.F. Gratton E, Time-resolved fluorescence emission spectra of laurdan in phospholipid vesicles by multifrequency phase and modulation fluorometry, Cell. Mol. Biol. 32 (1) (1986) 103–108.
[45] G. Bonaventura, et al., Laurdan monitors different lipids content in eukaryotic membrane during embryonic neural development, Cell Biochem. Biophys. 70 (2) (2014) 785–794.
[46] M.A. Digman, et al., The phasor approach to fluorescence lifetime imaging analysis, Biophys. J. 94 (2) (2008) L14–L16.
[47] D.M. Jameson, E. Gratton, R. Hall, The measurement and analysis of heterogeneous emissions by multifrequency phase and modulation fluorometry, Appl. Spectrosc. Rev. 20 (1984) 55–106.
[48] G. Redford, R. Clegg, Polar plot representation for frequency-domain analysis of fluorescence lifetimes, J Fluoresc 15 (2005) 805–815.
[49] A. Celli, et al., The epidermal Ca(2 +) gradient: measurement using the phasor representation of fluorescent lifetime imaging, Biophys. J. 98 (5) (2010) 911–921.
[50] S.et al. Sanchez, Alpha hemolysin induces an increase of erythrocytes calcium: a FLIM 2-photon phasor analysis approach, PLoS One 6 (6) (2011) e21127.
[51] N.G. James, et al., Applications of phasor plots to in vitro protein studies, Anal. Biochem. 410 (2011) 70–76.
[52] L.C. Chen, et al., Fluorescence lifetime imaging microscopy for quantitative biological imaging, Methods Cell Biol. 114 (2013) 457–488.
[53] F. Fereidouni, B.A, H.C. Gerritsen, Spectral phasor analysis allows rapid and reliable unmixing of fluorescence microscopy spectral images, Opt Express. 20 (12) (2012) 12729–127341.
[54] L. Malacrida, A.S, A. Briva, M. Bollati-Fogolín, E. Gratton, L.A. Bagatolli, Spectral phasor analysis of laurdan fluorescence in live A549 lung cells to study the hydration and time evolution of intracellular lamellar body-like structures, Biochim. Biophys. Acta. 1858 (11) (2016) 2625–2635.
[55] S.A. Sanchez, et al., A two-photon view of an enzyme at work: crotalus atrox venom PLA2 interaction with single-lipid and mixed-lipid giant unilamellar vesicles, Biophys. J. 82 (2002) 2232–2243.
[56] J.R. Lakowicz, Principles of Fluorescence Spectroscopy, 2nd ed., Kluwer Academic/Plenum Publishers, New York, London, Moscow, Dordrecht, 1999.
[57] M.S. Jaureguiberry, et al., Membrane organization and regulation of cellular Cholesterol homeostasis, J. Membr. Biol. 234 (3) (2010) 183–194.
[58] R.B. Macgregor, G. Weber, Estimation of the polarity of the protein interior by optical spectroscopy, Nature 319 (1986) 70–73.
[59] M. Stefl, N.G. James, D.M. Jameson, Applications of phasors to in vitro time-resolved fluorescence measurements, Anal. Biochem. 410 (2011) 62–69.
[60] J.E.a.J. Flores, The relative locations of intramembrane fluorescent probes and of the cytosol hemoglobin in erythrocytes, studied by transverse resonance energy transfer, Biophys. J. 37 (1982) 6–7.
[61] D.C.a.P.J. Jaromir Plasek, Fluidity of intact erythrocyte membranes. Correction for fluorescence energy transfer from diphenyihexatriene to hemoglobin, Biochim. Biophys. Acta 941 (1988) 119–122.
[62] J.Y. Nurith Shaklai, Helen M. Ranney, Interaction of hemoglobin with red blood cell membranes as shown by a fluorescent chromophore, Biochemistry 16 (25) (1997) 5585–5592.
[63] Brian M. Stott, M.P.V, Chisako O. McLemore, M. Shaun Lund, Elizabeth Gibbons, Taylor J. Brueseke, Heather A. Wilson-Ashworth, John D. Bell, Use of fluorescence to determine the effects of cholesterol on lipid behavior in sphingomyelin liposomes and erythrocyte membranes, J. Lipid Res. 49 (2008) 1202–1215.
[64] M. Faith, S.K.S. Harris, John D. Bell, Physical properties of erythrocyte ghosts that determine susceptibility to secretory phospholipase A2, J. Biol. Chem. 276 (25) (2001) 22722–22731.
[65] N. Becerra, et al., Characterization of micelles formed by sucrose 6-O-monoesters, Colloid Surface A 327 (1-3) (2008) 134–139.
[66] C. Toro, et al., Solubilization of lipid bilayers by myristyl sucrose ester: effect of cholesterol and phospholipid head group size, Chem. Phys. Lipids 157 (2) (2009) 104–112.